School of Computer Science and Engineering

Faculty of Engineering

The University of New South Wales

Stented Artery Computational Modelling

by

Vivian Bakiris

Thesis submitted as a requirement for the degree of

Bachelor of Engineering in Bioinformatics Engineering/ Master of Biomedical Engineering

Submitted:	July 2019	Student ID:	z5062431
Supervisor:	Dr. Susann Beier	Topic ID:	N/A

Abstract

Coronary Artery Disease (CAD) is the leading cause of death globally. Stenting is the most common form of treatment, and although highly effective, it continues to fail in approximately 160,000 patients anually. To better understand stent failure, this project aims to develop an anatomically correct computational model of a coronary artery from micro-CT output.

In order to address this issue, this investigation explores three key methodologies for doing so: growth, alignment and segmentation approaches. This work also proposes a novel methodology that incorporates aspects from the growth and alignment approaches. This final method is then evaluated in terms of its quality and ease of use.

Acknowledgements

I would like to acknowledge my supervisor Dr Susann Beier and my assessor Dr Sowmya Arcot for their guidance and support throughout my project. I would like to acknowledge Ramtin Gharleghi for his technical support and advice.

I would like to thank Laurence Boss for providing me with access to critical hardware during times of hardship.

Finally, I would like to thank Alan Shenfield for his continued and consistent support over the last four years of my degree.

Abbreviations

CPD Coherent Point Drift

CFD Computational Fluid Dynamics

CAD Coronary Artery Disease

CHD Coronary Heart Disease

DES Drug Eluting Stent

ICP Iterative Closest Point

Micro-CT Micro Computed Tomography

RMSE Root Mean Squared Error

STL File Stereolithography File

Contents

1 Introduction **1**

2 Background **3**

2.1 Coronary Artery Disease 3

2.2 Treatment 3

2.2.1 Stent Failure Mechanisms 4

2.2.2 Causes of Stent Failure 5

2.3 Bench Testing 5

2.3.1 Phantoms 5

2.3.2 Micro-CT 6

2.4 Model Development 7

2.4.1 Image Segmentation 7

2.4.2 Image Registration 7

2.4.3 Vessel Construction 8

2.5 Summary 10

3 Methods **11**

3.1 Segmentation 12

3.2 Growth 13

3.3 Alignment 15

3.4 Novel Approach 16
3.4.1 Pre-Processing 17
3.4.2 Alignment 20
3.4.3 Surface Construction 23
3.4.4 Post-Processing 24

4 Evaluation **25**

4.1 Assessment of Approaches 25
4.1.1 Segmentation Approach 25
4.1.2 Alignment Approach 25
4.1.3 Growth Approach 26
4.2 Assessment of Novel Approach 27
4.2.1 Pre-processing 27
4.2.2 Alignment 29
4.3 Assessment of Outcome 31
4.3.1 Quality 31
4.3.2 Ease of Use 32

5 Future Work **33**

6 Conclusion **34**

Bibliography **35**

Appendix A **39**

A.1 CPD Simulation Output 39
A.2 ICP Simulation Output 40

Appendix B **41**

B.1 Similarity Simulation 41

List of Figures

2.1 The Link Between Arterial Shape and Stent Failure 5

2.2 Vascular Reconstruction with Blender 9

3.1 STL file of vessel 11

3.2 STL file of stent 11

3.3 Segmentation Workflow 12

3.4 Segmentation Workflow Output 12

3.5 The Stages of the Growth Process. LHS: Alignment of simplified vessel and stent. RHS: Application of shrink wrap modifier. 13

3.6 Growth Approach Output 14

3.7 Iterative Closest Point Output. LHS: Vessel and stent alignment prior to ICP registration. RHS: Vessel and stent alignment following ICP registration. 15

3.8 Novel Approach Workflow 16

3.9 Left: STL File of Stent Pre-processed (1,500,000 vertices). Right: STL File of Stent Post-Process (1,500,000 vertices) 17

3.10 Vessel Prior to Processing 18

3.11 Exterior Wall of Vessel Selected for Removal 18

3.12 Vessel Post Processed 18

3.13 Stent Extension. LHS: Original Stent. RHS:Stent with additional extension. 19

3.14 Vessel and Stent Prior to Manual Alignment 20

3.15 Manual Alignment Output 20
3.16 Rigid Alignment Output 21
3.17 Coherent Point Drift Output 22
3.18 Surface Construction Output 23
3.19 Vessel Clipping with VMTK 24

4.1 Output of Previous Work 26
4.2 Output of Growth Approach 26
4.3 A comparison of the stent at different stages of denoising 28
4.4 CPD vs ICP 29
4.5 CPD Alignment following ICP and Manual Alignment 30
4.6 CPD Alignment without ICP and Manual Alignment 30
4.7 Comparison of CPD Alignment with and without previous alignment . . 30
4.8 Stent vs Vessel Similarity. A score of zero indicates a perfect match. . . 31
4.9 Workflow in terms of ease of use. 32

List of Tables

3.1 Input Parameters to ICP Algorithm 15

3.2 Input Parameters to CPD Algorithm 22

4.1 ICP Registration Times for a Range of Denoised Stents 27

Chapter 1

Introduction

Coronary Artery Disease (CAD) is the leading cause of death globally, responsible for 7.5 million deaths annually [3]. Thus, it is vital that effective treatment methods are developed and deployed. At the moment, angioplasty followed by stenting is the most common and effective form of treatment. Despite the success of this methodology, there is currently a 7% failure rate amongst all procedures [4]. These failures occur in the form of late stent thrombosis and restenosis.

Stent thrombosis and restenosis have been heavily associated with the damage of endothelial cells. These cells respond to changes in shear stress, that is caused by changing blood flow [15]. Although current research suggests a link between arterial shape, blood flow and therefore subsequent stent failure, there are few studies considering this.

In order to investigate this phenomenon, as well as determine an idealised stent implant technique for specific types of vessel shapes, a computational model must be developed for each group of vessels. Such a model would give way for both validation and testing of the connection between arterial shape and stent failure, as well as provide a model for assessing personalised stent implant techniques. The use of 3D printed phantoms will allow for different strategies for the same vessel.

This study investigated 3 methodologies for vessel reconstruction given two STL files as

input; one of a stent and one of a vessel prior to stenting. This work also presents a novel methodology that aims to produce the same outcome as the 3 proposed methods. The new methodology consists of 4 phases: data processing, alignment, surface construction and post-processing. Each stage of this process was analysed as well as their outputs in terms of quality and ease of use.

Chapter 2

Background

2.1 Coronary Artery Disease

Coronary Artery Disease (CAD), also known as Coronary Heart Disease (CHD), is responsible for approximately 1 in 4 deaths globally, making it the leading cause of death in the world [3]. CAD involves the narrowing of arteries, typically caused by a build up of plaque on the arterial wall (atheroma). This ultimately results in the reduction of blood flow, often resulting in myocardial infarction.

There are several known risk factors associated with CAD, including high blood pressure, high cholesterol, diabetes and obesity [44]. Each of these factors have displayed an increased prevalence in society, thereby increasing the urgency of developing effective methods of treatment for CAD [22].

2.2 Treatment

To combat the effects of CAD, angioplasty is performed followed, by stenting. Angioplasty involves a balloon catheter being inserted at the site of the blocked artery. Following this, the balloon is inflated to restore the blood flow through the affected

vessel. Simultaneously, a cylindrical wire mesh, known as a stent, is inserted. This stent assists with promoting blood flow by keeping the artery open [29].

Originally, angioplasty was preformed without the addition of a stent, however this often led to severe complications, such as myocardial infarction as a result of elastic recoil. The incidence of elastic recoil following angioplasty saw significant reductions following the introduction of stenting [23].

The first type of stents implanted were bare metal stents, although, patients with these stents often experienced a high incidence of stent thrombosis and were at risk of in-stent restenosis, occuring in 20-30% of cases (see Section 1.3) [23]. To counter this issue, the Drug-Eluting Stent (DES) was developed. A DES is designed to allow the release of chemicals to the local surrounding tissue, which prevents the progression of many of the complications associated with bare metal stents [20].

2.2.1 Stent Failure Mechanisms

Despite the introduction of the DES, the use of stents continues to fail in 160,000 patients annually [4]. This failure takes the form of in-stent restenosis and late stent thrombosis.

In-stent restenosis In-stent restenosis, which causes the lumen diameter to shrink, is a product of the migration and proliferation of vascular smooth muscle cells within the stents [23]. The main cause of restenosis is neointimal hyperplasia. Neointimal hyperplaysia is the main process of vascular repair, whereby the intimal layer of the artery is thickened [14], causing a further narrowing of the arteries and reduction of blood flow.

Late Stent Thrombosis Late stent thrombosis is the formation of a blood clot in a vessel and has an incidence of around 0.5-2% [28]. The implications of this are

significant as late stent thrombosis results in myocardial infarction in 70% of cases [19, 20].

2.2.2 Causes of Stent Failure

The damage of endothelial cells have been associated with late stent thrombosis, and the subsequent stent failure [15]. Endothelial cells are a layer of cells that line the walls of blood vessels [1]. These cells play a significant role in suppressing inflammation and thrombosis as well as controlling vascular tone and function.

Endothelial cells actively respond to the shear stress created by phasic blood flow [37]. Studies have shown that the sheer stresses that occur as a result of stent implantation results in the damage and loss of such cells [15, 17].

As highlighted in Figure 2.1, there is a suggested connection between arterial shape and stent failure. As shear stress is created and modified by blood flow, and arterial shape affects blood flow, it can therefore be suggested that arterial shape is a factor in stent failure. Despite this link, there are few studies which consider this phenomenon.

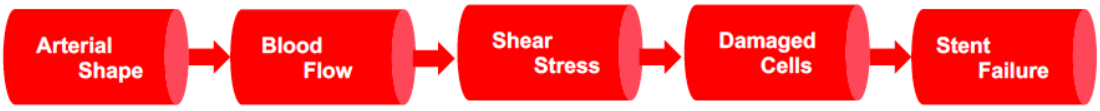

Figure 2.1: The Link Between Arterial Shape and Stent Failure

2.3 Bench Testing

2.3.1 Phantoms

Phantoms, in the space of medical imaging, are manufactured/synthetic objects used as replicas for human tissue. Traditionally, phantoms have been used to validate imaging techniques [34]. As phantoms are created to mimic the human tissue response in particular conditions, there are further applications to their use. Their properties include

their strength and durability designed to withstand physiological pressures as well as their elastometric properties that are similar to vascular tissue. These properties make phantoms ideal for modelling stent implantation, and multiple studies have utilised them for clinical assessments [21, 35, 38].

Recent advancements have seen the introduction of 3D printing as a viable method of manufacturing phantom models [21]. Phantoms are therefore able to replicate human tissue response and can be highly customised through 3D printing. These characteristics make the use of phantoms a desirable option for modelling stent implantation, specifically when considering arterial shape on a patient by patient basis.

2.3.2 Micro-CT

Micro Computed Tomography (Micro-CT) is a non destructive technique that produces 3D images, including internal structures, of a sample [36]. Micro-CT can be utilised to create a series of 2D cross sections of arterial structures to provide a direct reconstruction of the internal and external vessel geometry [32]. This technique is often considered the "gold standard" in the medical imaging community, as highlighted in Cosentino et. al (2014), in a study where imaging techniques for the 3D reconstruction of stent geometry are assessed.

Micro-CT has been widely used to reconstruct anatomically correct models of blood vasculature [7, 11, 16]. However, studies have shown that when micro-CT has been used in a phantom study of in-stent restenosis, there are visualisation complications. In particular, the presence of the stent creates blooming artefacts, causing a lower spatial resolution and spatial deterioration in the image quality [35]. Such effects make it difficult to visualise the vasculature and stent simultaneously.

2.4 Model Development

2.4.1 Image Segmentation

Most studies that create computational models using micro-CT images utilise image segmentation, which involves the separation of an image into components with shared properties [7, 11, 16, 42]. Recent advancements in image segmentation have resulted in the extraction of the surfaces of structures from 3D medical imaging data [10]. However, while 3D modeling based off micro-CT images has been widely used and implemented, micro-CT techniques cannot simultaneously detect biological and metallic surfaces, as described in Section 2.1.2. This holds true for all current major imaging techniques [32].

2.4.2 Image Registration

Image registration is a process in which two images are overlaid and geometrically aligned for image analysis [26]. Image registration allows for the correlation of structural changes between two inputs. The process of image registration produces a population image (the overlaid and aligned images together) as well as several statistical outputs. One such category of statistical outputs are similarity metrics, which provide a quantitative evaluation of the similarity between inputs. A study conducted by Penney et al (1998) investigated several of these similarity metrics. In this study, a comparison of similarity measures was conducted with a CT scan of a spine phantom, and concluded the most effective metric was pattern intensity [38]. Thus, this metric will be utilised for this project.

There are several different image registration algorithms and methods. The two that this study will be investigating are Iterative Closest Point and Coherent Point Drift.

Iterative Closest Point The Iterative Closest Point (ICP) algorithm is regarded as the most prominent method for aligning 3D models using geometric properties.

The algorithm begins with two input point clouds as well as an estimation for their relative body transformation. The ICP algorithm then iteratively refines the transform by repeatedly generating pairs of corresponding points, seeking to minimise an error metric [43].

Coherent Point Drift Coherent point drift is a probabilistic method of image alignment. It is a registration algorithm based on the Gausian Mixture Model (GMM) and uses an Expectation Maximisaion scheme [25]. It considers the alignment of two point sets as a probability density estimation problem [33]. The algorithm is robust to outliers as well as noise. This method is effective for registration in multiple dimensions [25] and has therefore been utilised and adapted to perform image registration in the processing of medical images [39]. One key limitation of the CPD algorithm is that of it's convergence rate being inversely related to the size of the input, as a result of the EM scheme [25].

2.4.3 Vessel Construction

Idealised vessels are frequently constructed for use in Computational Fluid Dynamics (CFD). There are several tools and frameworks in use for vessel construction and modification, including the Vascular Modelling ToolKit, MeshLab and Blender.

Vascular Modelling ToolKit The Vascular Modelling Toolkit (VMTK) is an open-source image based framework for patient-specific computational haemodynamics. VMTK integrates image processing, geometric analysis and mesh generation techniques to create personalised vascular models [2]. The capabilities of the VMTK include, but are not limited to, vascular smoothing which implements a Taubin filter, surface clipping and the addition of flow extensions [40]. The VMTK is used extensively in the space of cardiovascular research, particularly for use in CFD [6, 18, 27, 41, 45].

MeshLab MeshLab is an open-source 3D mesh-processing tool with a range of embedded features including Simplification, Surface Construction, Smoothing and Normal Calculation [13]. One such simplification tool within meshlab is Quadric Edge Collapse Decimation. This method simplifies the mesh in the following way: an edge (two joining vertices) is collapsed into a single vertex, then the two faces between the edge are removed [31]. Poisson surface reconstruction is another tool offered within MeshLab. This tool expressed reconstruction as the solution to a Poisson equation, reconstructing a watertight triangulated approximation to a surface [24].

Blender Blender is a surface rendering software that can produce high quality animations of 3D models and data, which has been successfully applied in medical contexts [5, 9]. The use of blender to recreate the surrounding vasculature around an implanted stent has been partially implemented within Beier et al (unpublished). Within this study, a 3D model of the artery was developed and scanned with a micro-CT machine. These images were then converted to an STL file, thereby obtaining a file containing the blood vessel before implantation. Following this, the phantom was stented and scanned to generate another STL file. This produced a 3D reconstruction of the implanted stent, which was then used as an input into Blender, and the surrounding vasculature was recreated (see Figure 2.2). While this method has shown promising results, the implementation was not completed. The results, displayed in Figure 2.2, reveal opportunity for further development, particularly in smoothing the surrounding vasculature.

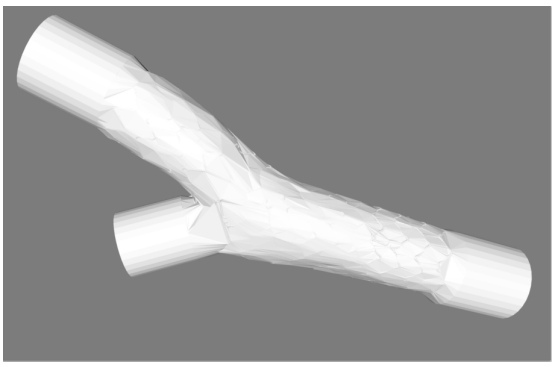

Figure 2.2: Vascular Reconstruction with Blender

2.5 Summary

There is a imperative need to determine the cause of stent failure, as CAD is the largest cause of death worldwide. In Section 2.2.2, this report highlighted the relationship between arterial shape and the effectiveness of stent implantation. However, assessment of current research in this chapter reveals that despite the likelihood that individual arterial shape influences stent implantation, there are a limited number of studies which consider it. Additionally, current methods do not focus on capturing vessel deformation due to the presence of the stent.

This chapter highlights several barriers to conducting a study of this nature. Notably, the inability to simultaneously visualise vasculature and stent from an image based computational modelling approach.

In order to determine the effect of individual coronary shape differences on stent implant success, a study of this kind must be conducted. This will determine if there is an ideal stent implantation technique for patient shapes. The use of 3D printed phantoms will allow for different strategies for the same vessel.

Chapter 3

Methods

The following chapter will describe the methods undertaken as well as demonstrate the results output from each methodology. An assessment of each method and output is described in Chapter 4. A 3D printed model of a vessel underwent stenting, this 3D printed phantom model was scanned by a Micro-CT machine prior to stenting as well as post stenting. The STL outputs of this imaging will serve as the input to each method. The resulting inputs consist of a STL file of a sample stent Figure 3.2, and an STL file of a vessel prior to stenting Figure 3.1.

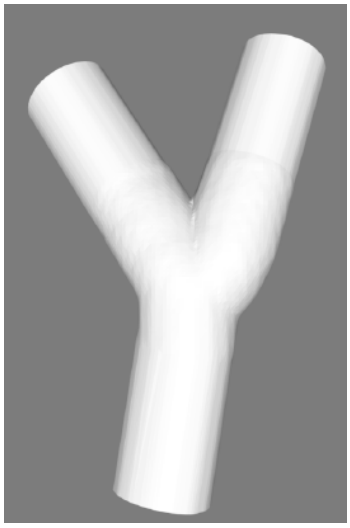

Figure 3.1: STL file of vessel

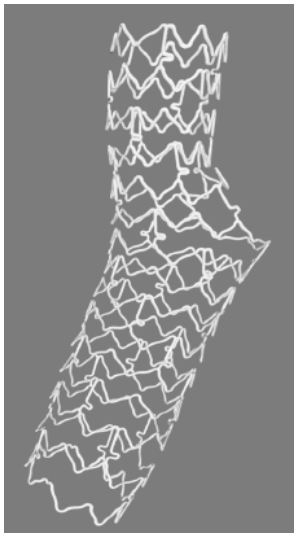

Figure 3.2: STL file of stent

3.1 Segmentation

The segmentation approach is conducted before the STL file is created. This method, as displayed in Fig 3.3 requires a set of DICOM files as input, which will be converted to an appropriate NRRD file using 3D Slicer, a medical image processing software tool. Following the conversion using 3D Slicer, the new NRRD file will be used as input into Seg3D, a segmentation tool. The implementation of this pipeline was haulted at the first stage of the implementation as a result of the dataset. Fig 3.4 presents one slice of the DICOM file. Three white markings are present, which represent the stent.

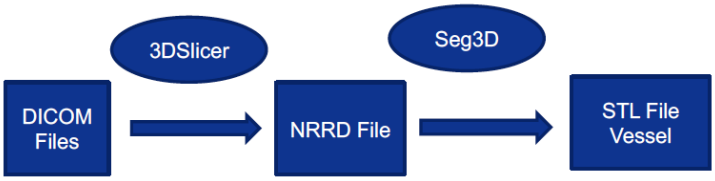

Figure 3.3: Segmentation Workflow

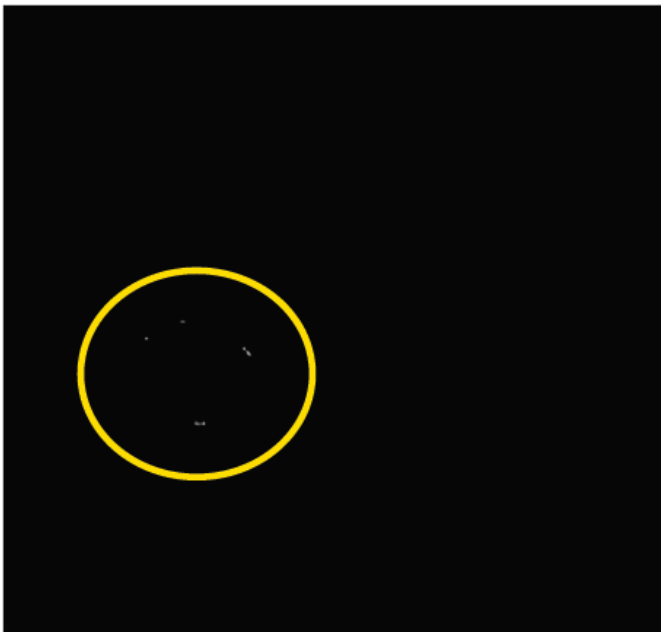

Figure 3.4: Segmentation Workflow Output

3.2 Growth

This growth approach continues to further develop the work established by Beier et al, described in Section 2.4.3. Given an STL file and the Blender software, this approach will utilize the shrink wrap tool to improve the current model. This tool, which can be applied to meshes, lattices, curves and surfaces, allows an object to shrink to the surface of another [8]. The use of this tool may successfully recreate the tissue of the vasculature surrounding the stent.

The growth approach requires the user to first import both the vessel and stent into the software. This is followed by simplification of the vessel, manual alignment of the simplified vessel and the original stent and finally the application of the shrink wrap modifier. These stages are demonstrated in Figure 3.5. The output of following this method is displayed in Figure 3.6 and further evaluated in Section 4.1.3.

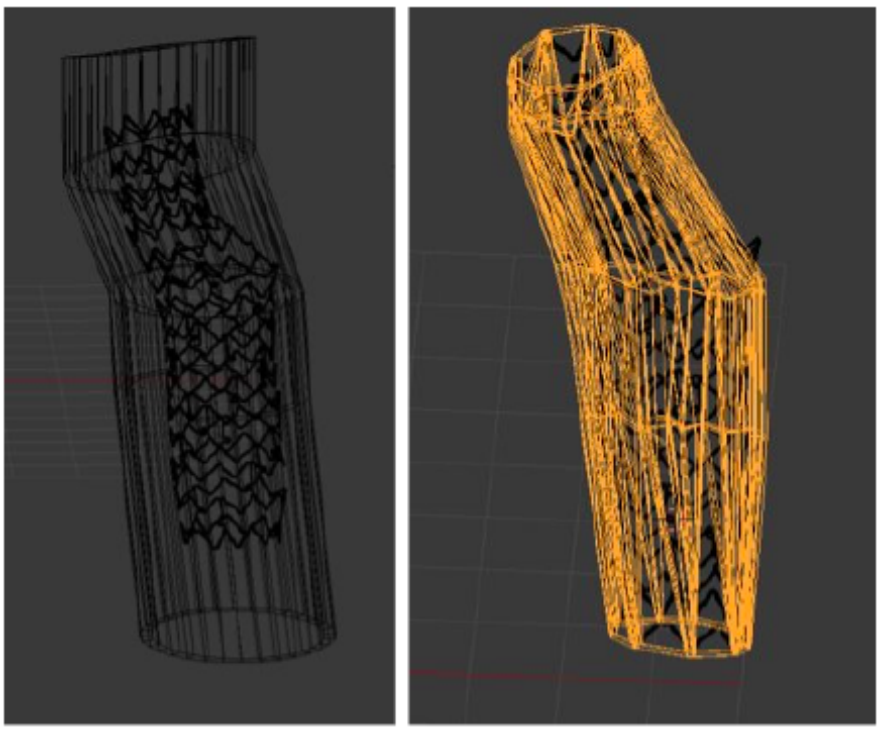

Figure 3.5: The Stages of the Growth Process. LHS: Alignment of simplified vessel and stent. RHS: Application of shrink wrap modifier.

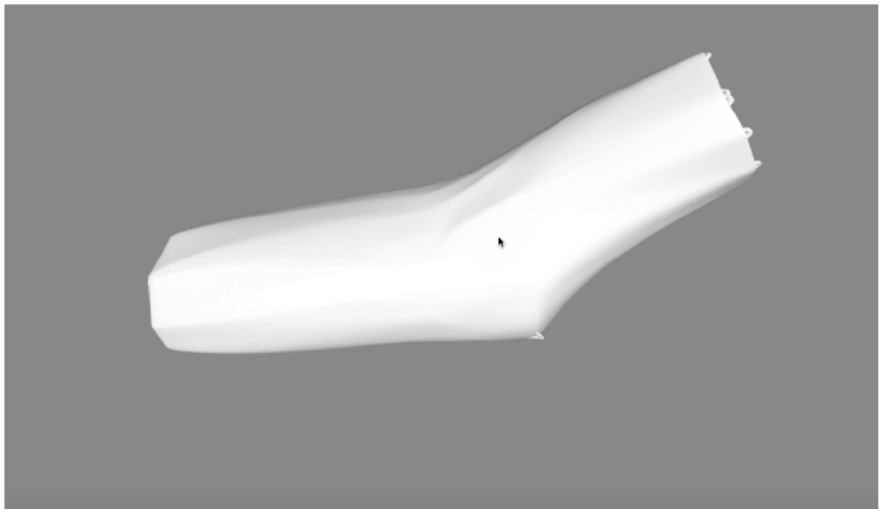

Figure 3.6: Growth Approach Output

3.3 Alignment

The alignment approach utilises the STL file of the stent (See Figure 3.2) and the STL file of the vascular pre-stenting (See Figure 3.1). This method aims to register Figure 3.2 and Figure 3.1 via implementation of the Iterative Closest Point algorithm as described in Chapter 2.4.2. Given the two aforementioned inputs, the ICP algorithm was implemented via MatLab. The algorithm was executed with the parameters outlined in Table 3.1, with the output demonstrated in Figure 3.7.

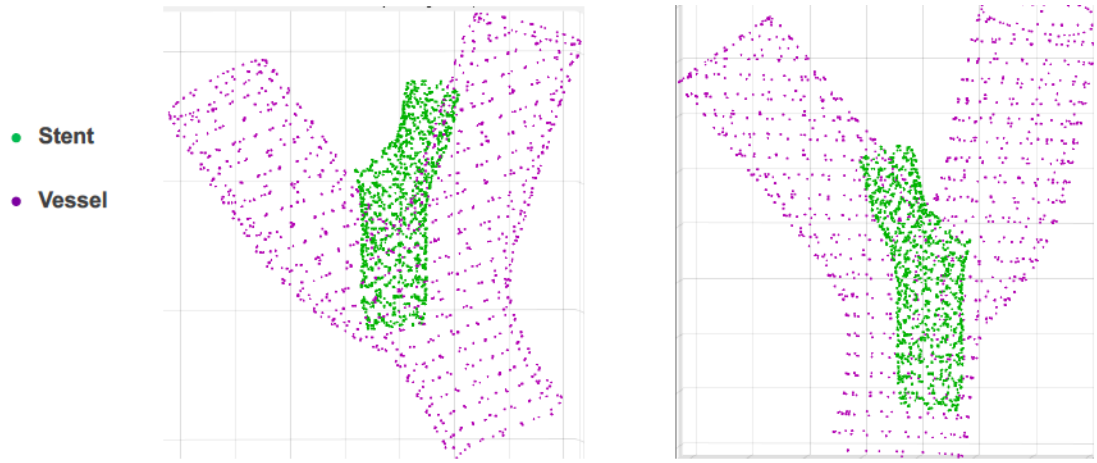

Figure 3.7: Iterative Closest Point Output. LHS: Vessel and stent alignment prior to ICP registration. RHS: Vessel and stent alignment following ICP registration.

Parameter	Range	Selected Value	Reason
Metric	Point to Point or Point to Plane	Point to Plane	Point to plane is more suitable for non-planar inputs
Iterations	Scalar	15	After 15 iterations changes to output plateau and therefore further iterations are not required.
Tolerance	Two Scalars	0.01,0.009	Default parameters set. Altering parameters has no impact on output.

Table 3.1: Input Parameters to ICP Algorithm

3.4 Novel Approach

Over the course of this thesis, a novel methodology was developed that aimed to reconstruct a vessel wall post-stenting. This method, as described in Figure 3.8, involved 4 key stages: Pre-processing, Alignment, Surface Construction and Post-Processing. The following section will describe each of the 4 key stages as well as describe the final output.

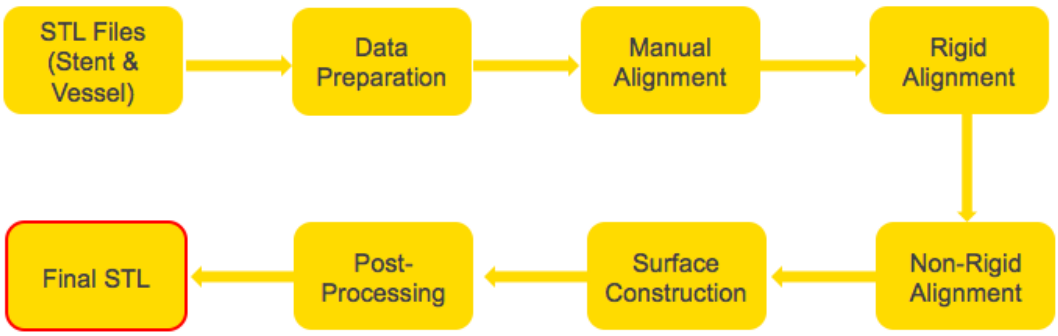

Figure 3.8: Novel Approach Workflow

3.4.1 Pre-Processing

Data Downsampling

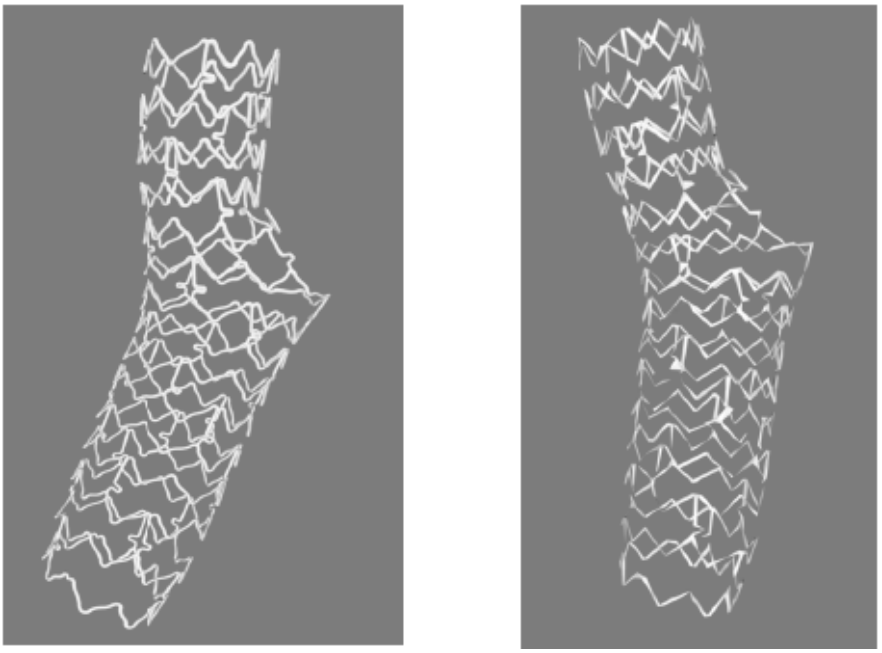

Figure 3.9: Left: STL File of Stent Pre-processed (1,500,000 vertices). Right: STL File of Stent Post-Process (1,500,000 vertices)

One of the key limitations to the dataset is the sheer size of the files (151.6MB), as the stent had 9,096,042 vertices. The number of vertices resulted in low performance in all previously explored methods. To enhance the performance of the algorithm, the stent was simplified.

The STL file of the stent was imported into MeshLab and duplicated vertices were unified. This resulted in a decrease from 9,096,042 to 1,515,844 vertices, whereas the number of faces remained the same at 3,032,014.

The Quadric Edge Collapse Decimation algorithm was subsequently applied with the following parameters - Preserve Normals, Preserve Topology, Preserve Boundary of Mesh and Optimal Position of Simplified Vertices. Using this method the stent was simplified to 1,506 vertices.

Vessel Simplification

The vessel was simplified, by removing the outer wall. As shown in Fig 3.10, the original STL vessel file consists of both an interior and an exterior wall, representing the inner lumen and the outer vessel. Vessel simplification is conducted using the Blender modelling software. All external vertices are selected and subsequently decimated, resulting in the inner wall of the vessel remaining.

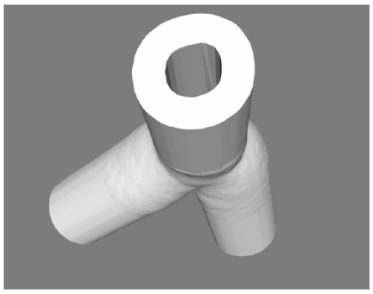

Figure 3.10: Vessel Prior to Processing

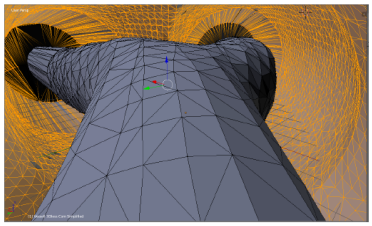

Figure 3.11: Exterior Wall of Vessel Selected for Removal

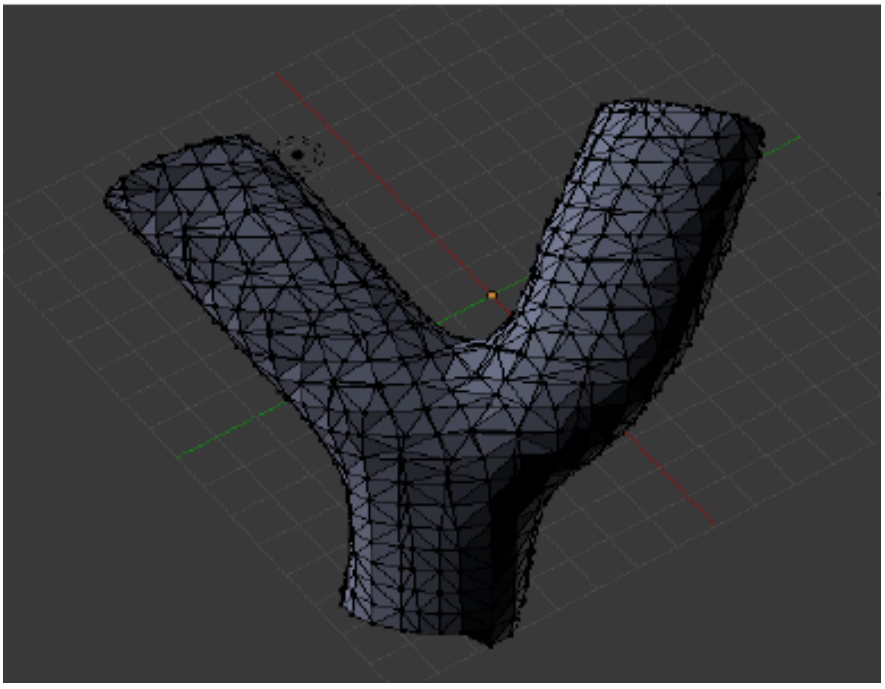

Figure 3.12: Vessel Post Processed

Stent Extension

The final stage in the data pre-processing phase is to perform stent extension. This step is executed in the modelling software Blender, as described in Section 2.4.3. As displayed in Fig 3.13, an additional appendage is added using the cylindrical shape. This figure, in combination with the stent, is exported as one STL file, which is the new input to replace the original stent seen in Figure 3.2.

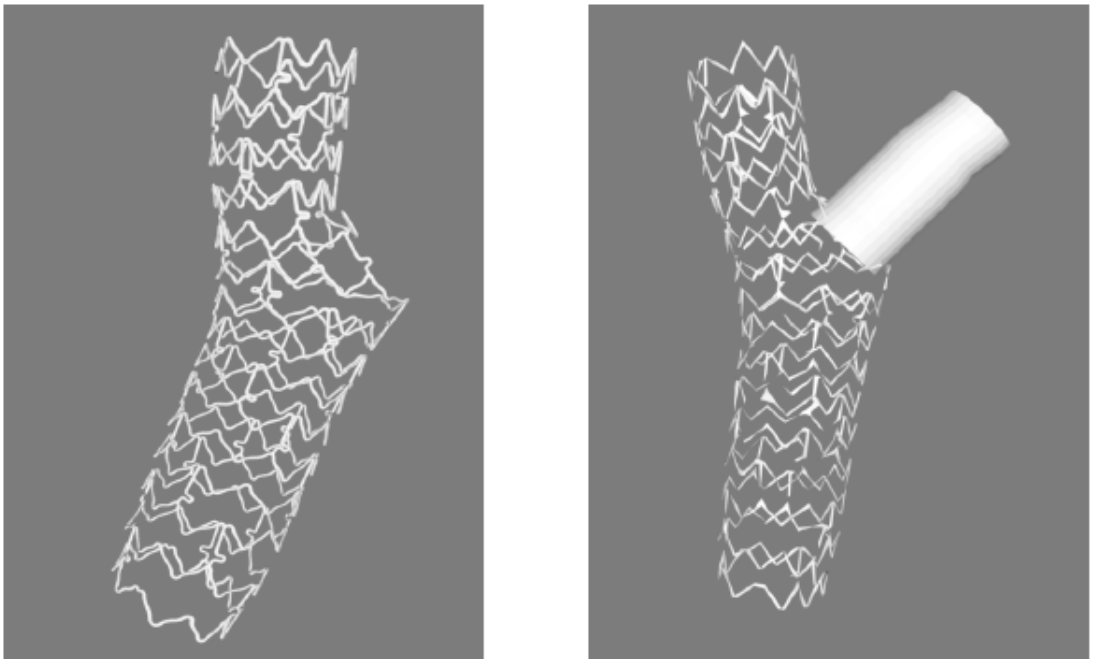

Figure 3.13: Stent Extension. LHS: Original Stent. RHS:Stent with additional extension.

3.4.2 Alignment

The alignment phase consists of three critical stages to produce the most accurate output. The first is a manual alignment, followed by a rigid registration and a non-rigid registration.

Manual Alignment

The first stage of alignment is manual. Manual alignment occurs through a series of scaling, rotation and transformation, and was conducted in Blender.

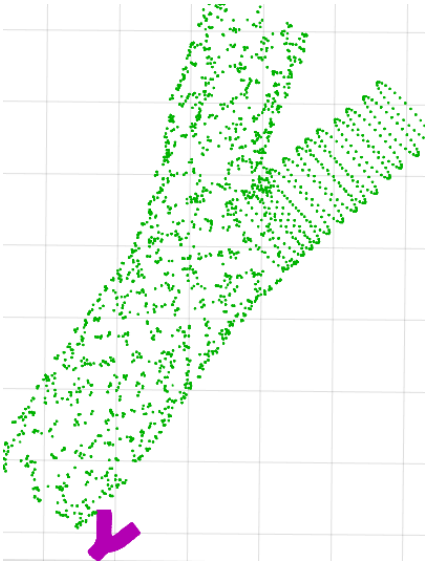

Figure 3.14: Vessel and Stent Prior to Manual Alignment

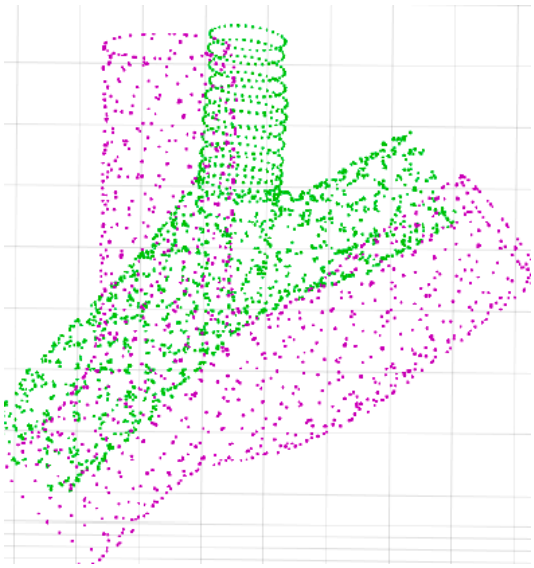

Figure 3.15: Manual Alignment Output

As displayed in Figure 3.15, the resulting transformation results in a more realistic alignment.

Rigid Registration

The next stage in the alignment process is rigid alignment through the ICP algorithm as described in Section 2.4.2.

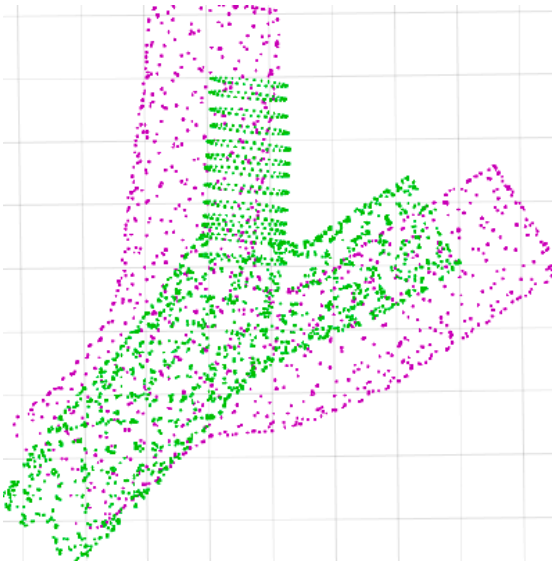

Figure 3.16: Rigid Alignment Output

Non-Rigid Registration

The final stage of the alignment phase is the implementation of the CPD Algorithm, as described in Section 2.4.2. The algorithm was implemented in MatLab, with the Figure 3.13 and Figure 3.12 as input, and parameters described in Table 3.2.

Parameter	Range	Selected Value	Reason
Transform	Rigid, Non-Rigid, Affine	Non-Rigid	Rigid performs akin to ICP. Affine does not maintain vessel shape.
Iterations	Scalar	45	After 45 iterations changes to output plateau and therefore further iterations are not required.
Tolerance	Scalar	1.00e-05	Default parameters set. Altering parameters has no impact on output.
Outlier Ratio	Scalar	0.9	Maximum Selected as the scalar reduces the impact of noise and outliers.

Table 3.2: Input Parameters to CPD Algorithm

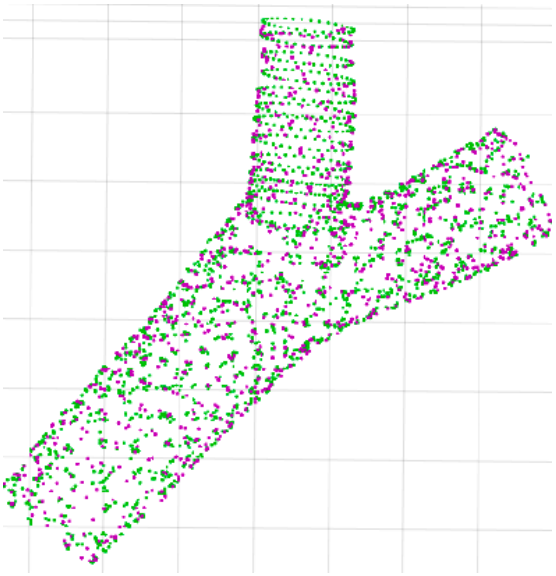

Figure 3.17: Coherent Point Drift Output

3.4.3 Surface Construction

The final point cloud is exported from MatLab into MeshLab. The normals are recalculated using the 'compute normals for point sets' filter. Given the input point cloud with the computed normals a surface is built utilising screened poisson reconstruction as described in Section 2.4.3.

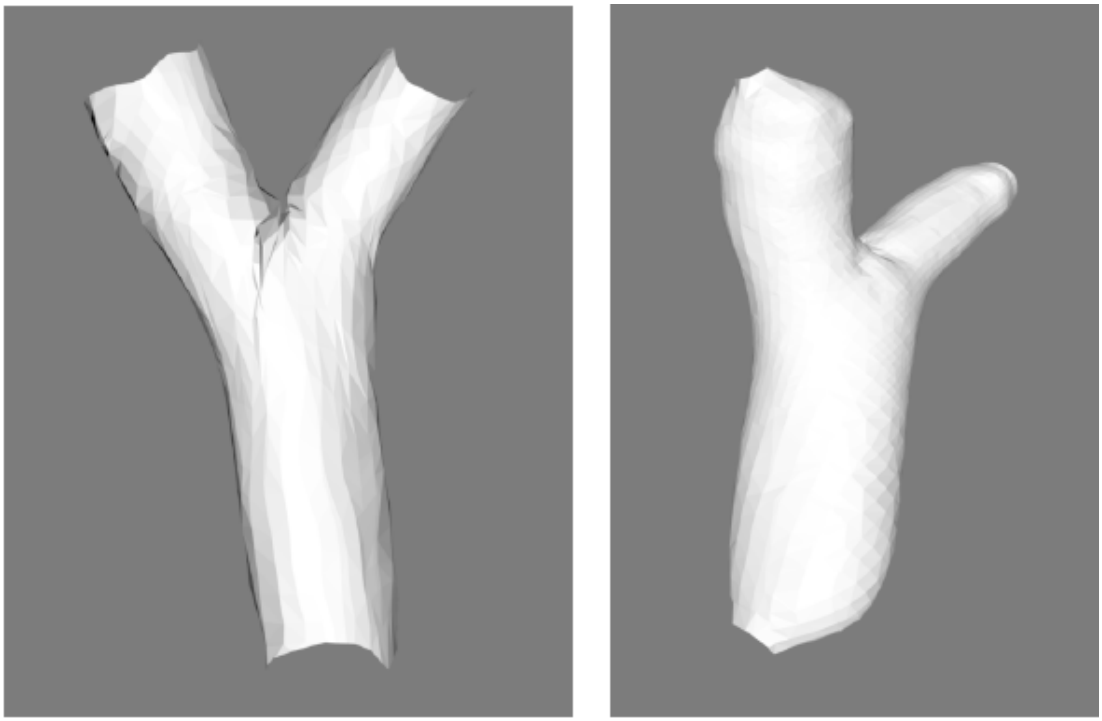

Figure 3.18: Surface Construction Output

3.4.4 Post-Processing

The final stages of this pipeline include post-processing of the output vessel. As demonstrated in Figure 3.18, there are some irregularities that arise from the vessel reconstruction phase, and the post processing aims to correct for these irregularities.

Vessel Cutting and Smoothing

The output vessel is modified by the VMTK Toolkit, described in Section 2.4.3. The 'closing in' of vasculator occured following surface reconstruction. In order to combat this, the vessel undergoes clipping. The vessel cutting pipeline is applied to remove the ends of the vessel, which will allow for blood flow in future CFD analyses.

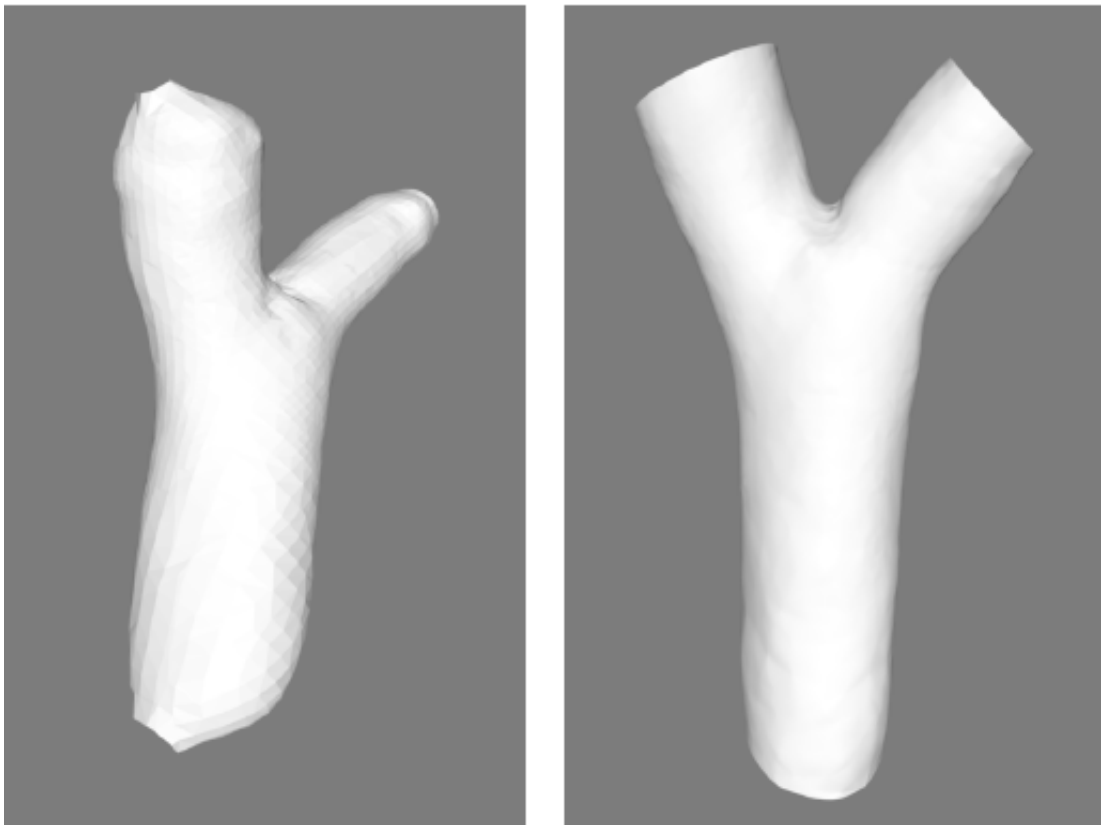

Figure 3.19: Vessel Clipping with VMTK

Chapter 4

Evaluation

This section presents an evaluation of each step in the method. This includes reflecting on why each stage was incorporated, the parameters selected, and the final result.

4.1 Assessment of Approaches

4.1.1 Segmentation Approach

The results shown in Fig 3.4 highlight the quality of the resulting DICOM files produced from the micro-CT of the stented vessel. The only visible elements are that of the stent. The resolution of the micro-CT machine is too low to detect the vessel lumen and the stent simultaneously. As a result, the pipeline proposed in Fig 3.3 is not feasible.

4.1.2 Alignment Approach

Section 2.2 highlights that through the process of stenting, the occluded blood vessel is deformed to allow the passage of blood. As the alignment approach utilising the ICP algorithm is rigid, the shape of the vessel is not deformed in the alignment in relation

to the stent. Therefore the produced output is not an accurate reconstruction of the stented vessel, and remains almost identical to the input vessel.

4.1.3 Growth Approach

One of the fundamental criteria of the produced vessel is the 'air-tight' of the mesh is as it will be used in CFD in future. The growth approach is a continuation of the unpublished work of Beier et al, displayed in Fig 4.1. Examining the mesh produced in Fig 4.2 by the growth approach in comparison to the mesh previously produced, clearly reveals that the overall quality of the mesh improved. When considering the number of manifold edges, Fig 4.1 contains 6,507 whereas Fig 4.2 contained 0. This indicates that the vessel produced is therefore of higher quality. Although the vessel performs quantitatively, a qualitative assessment reveals that the structure is not ideal. The bifurcated nature of the vessel is lost in this method, and therefore it is not a viable solution.

Figure 4.1: Output of Previous Work

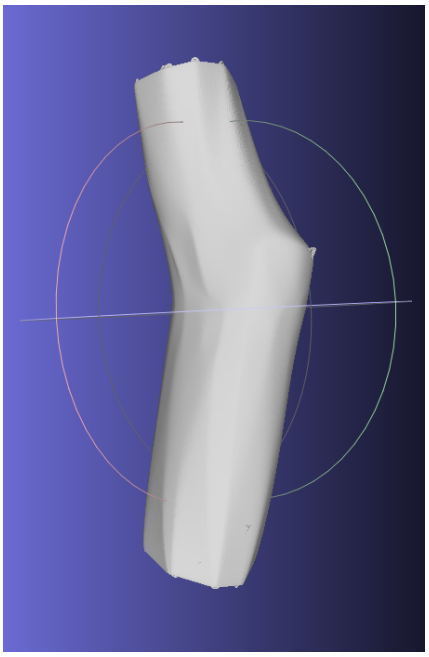

Figure 4.2: Output of Growth Approach

4.2 Assessment of Novel Approach

4.2.1 Pre-processing

The pre-processing phase evolved over the course of this study, as a response to the several barriers encountered during the implementation of Section 3.1 and Section 3.2, including memory, run-time and algorithm performance. The parameters of the down-sampling phase were selected as a trade off between efficiency and quality. The original stent STL file consisted of 1,500,000 vertices as displayed in Fig 3.9. Given the constraints of the CPD algorithm as described in Section 2.4.2, an input file of this size was not feasible. The process in determining the optimal number of vertices was iterative, as highlighted in Table 4.1. The file was iteratively down-sampled and input into a simple ICP pipeline until a viable number of vertices was determined. Following this, quality was then considered to determine the optimal surface. As demonstrated in Fig 4.3, the stent rings were examined qualitatively, in terms of their 'connectedness', in order to determine the appropriate number of vertices.

Number of Vertices	ICP Registration Time (s)
1,000	32
10,000	75
20,000	140
50,000	265
100,000	Failed
200,000	Failed
500,000	Failed
1,500,500	Failed

Table 4.1: ICP Registration Times for a Range of Denoised Stents

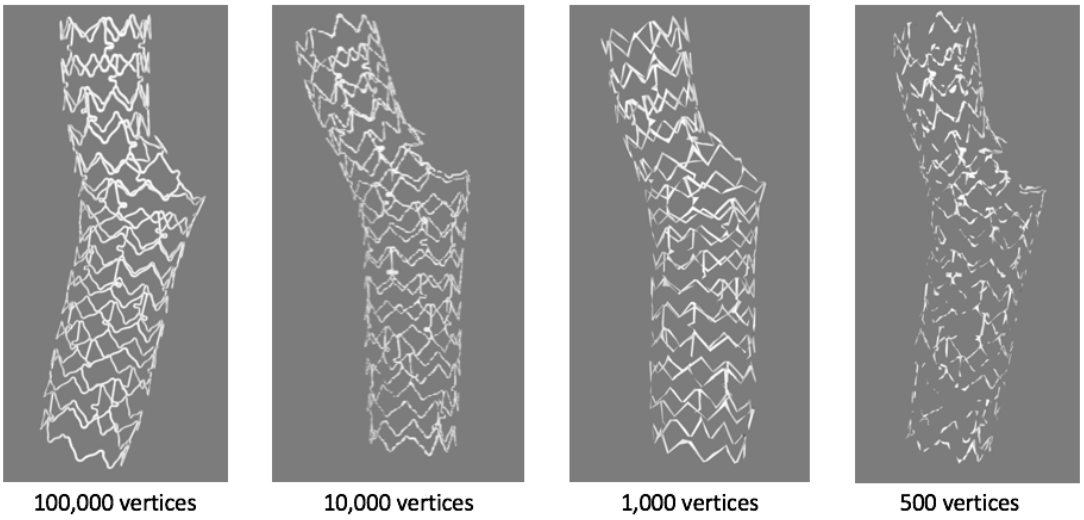

Figure 4.3: A comparison of the stent at different stages of denoising

4.2.2 Alignment

Three stages of alignment were chosen, as they achieved the best results. The RMSE was calculated between the vessel and the original stent to highlight the similarity between the two. From 4.4 it is clear that the CPD Algorithm performed better than the ICP algorithm. From 4.7 it can be shown that the optimal performance of the CPD algorithm is obtained following previous alignment. Therefore, 3 stages of alignment is more efficient, as it produces a better result with less required iterations.

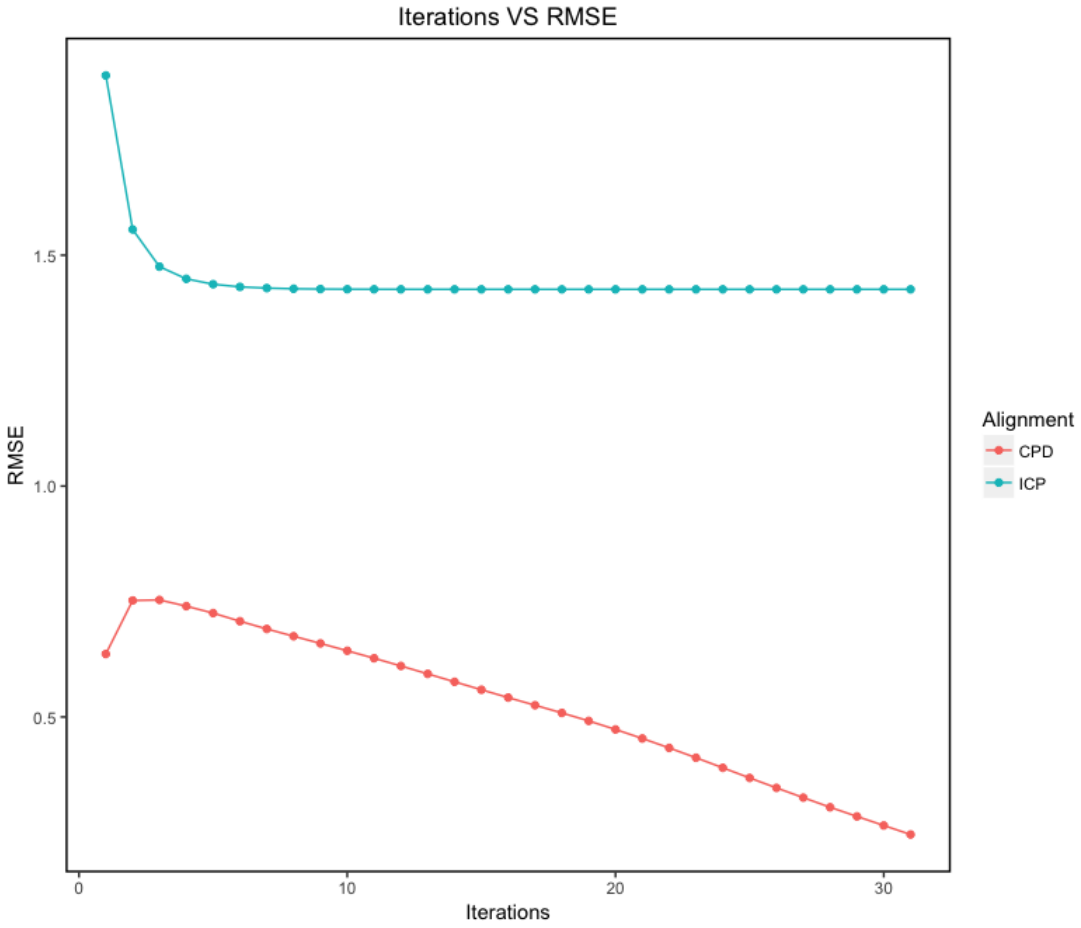

Figure 4.4: CPD vs ICP

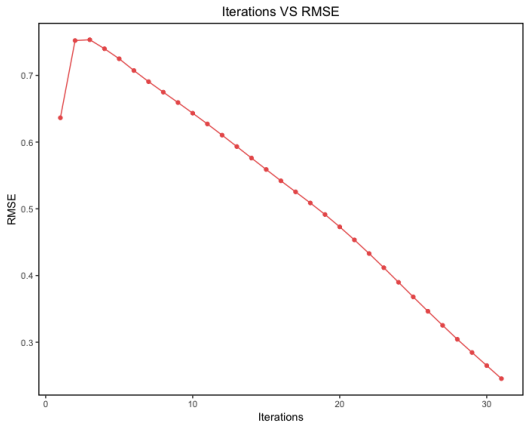

Figure 4.5: CPD Alignment following ICP and Manual Alignment

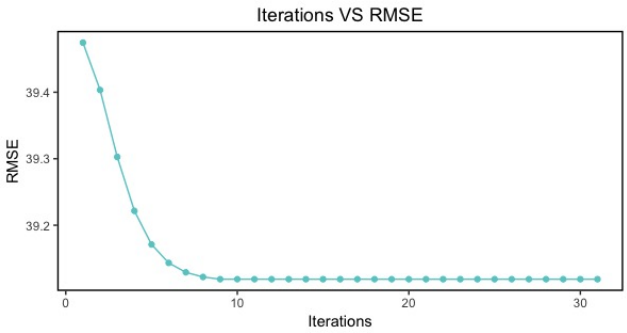

Figure 4.6: CPD Alignment without ICP and Manual Alignment

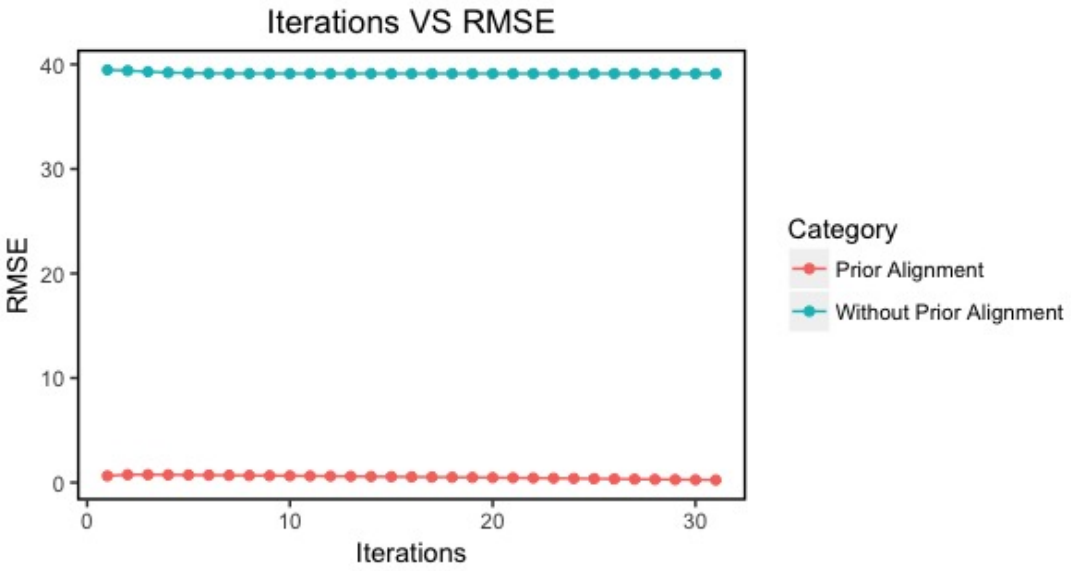

Figure 4.7: Comparison of CPD Alignment with and without previous alignment

4.3 Assessment of Outcome

4.3.1 Quality

The key limitations of the alignment and growth approaches explored in Sections 3.3 and 3.2 respectively are the extent of deformation of the produced vessel. In the case of Section 3.3, as the vessel was rigidly registered to the stent, the output was too similar to the original vessel (i.e. it had not deformed appropriately). In the case of Section 3.2, the vessel had deformed in excess, resulting in an output that was too dissimilar to the original vessel. The output quality of the novel method was assessed comparing two variables: stent similarity and vessel similarity. As demonstrated in Figure 4.8, the output of the novel approach out-performed all other methods and improved on the initial input.

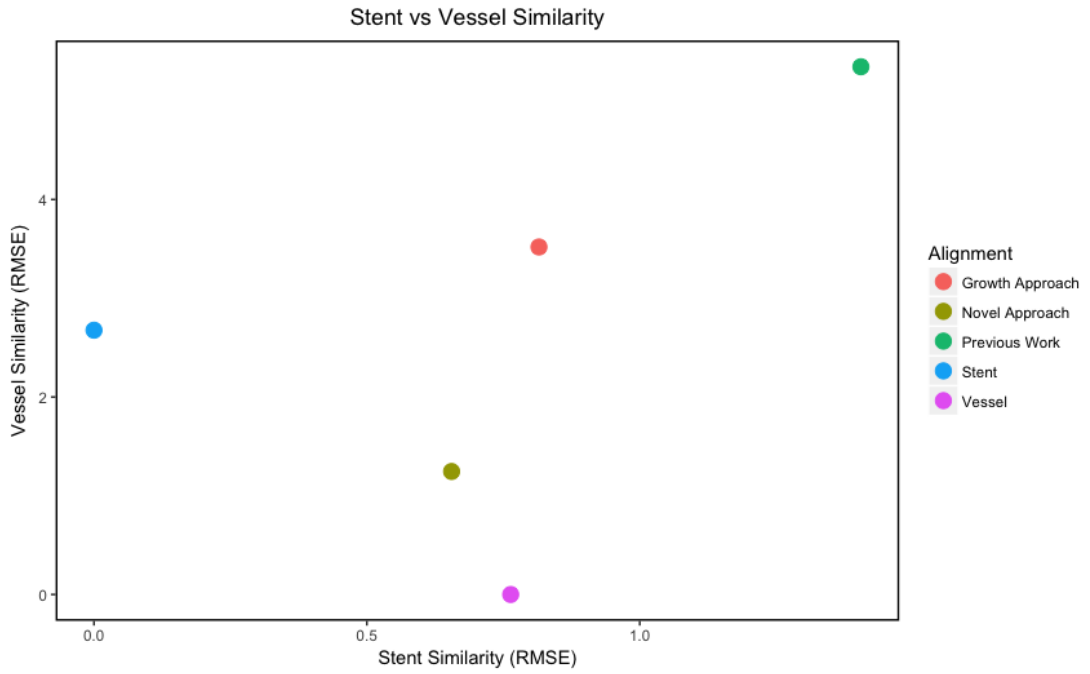

Figure 4.8: Stent vs Vessel Similarity. A score of zero indicates a perfect match.

4.3.2 Ease of Use

As the aim of this study is to ultimately deploy this pipeline to a large data set of patient specific vessel groups, ease of use is a significant consideration. Throughout the 10 stages of the pipeline, 20% required manual intervention, 20% required one stage of intervention, and 60% of the stages were automated. This is a significant improvement on the previous work described in Section 2.4.3, in which the entire methodology required human intervention.

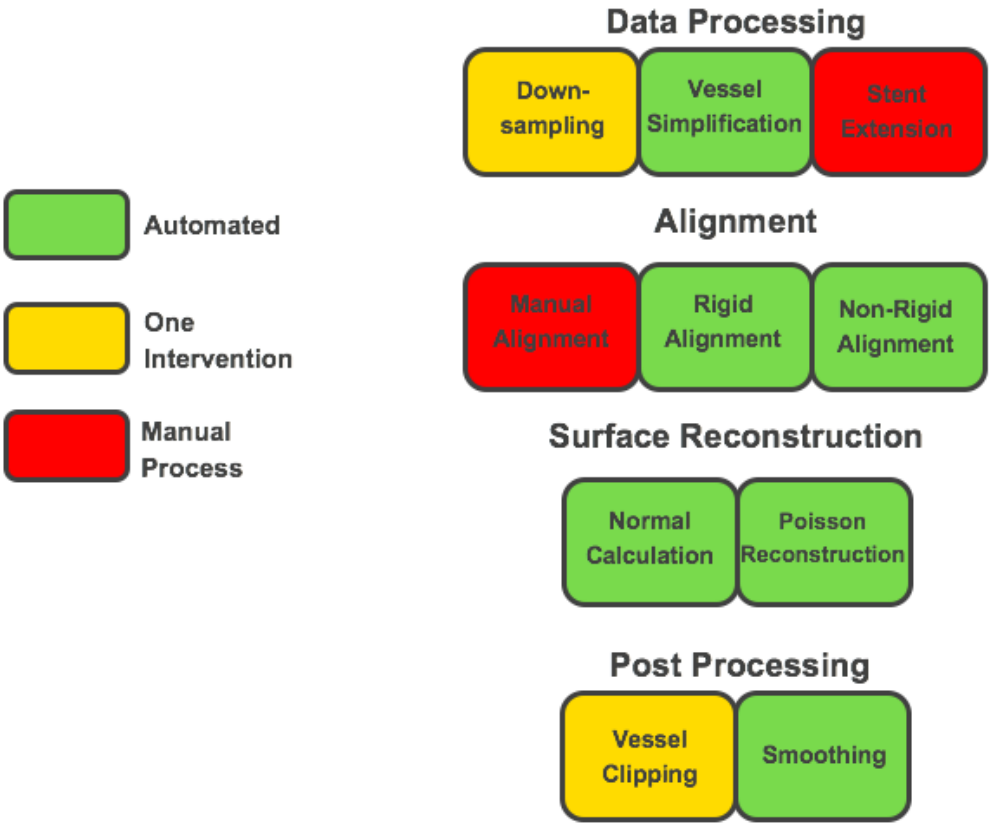

Figure 4.9: Workflow in terms of ease of use.

Chapter 5

Future Work

The developed pipeline will undergo further testing with multiple data sets to allow for further evaluation and assessment. Following this, the proposed methodology can be implemented on a larger data-set.

The key limitation of this work is that it lacks a 'gold-standard'. Industry standard for vascular reconstruction is the use of micro-CT as the 'ground-truth' 2.3.2. However, as described in Section 3.1, the use of micro-CT as a gold-standard is not feasible. As such, a new standard should be developed. Recent studies suggest the Optical Coherent Tomography (OCT) imaging technique can overcome the barriers posed by the micro-CT technology [30, 12]. This research opens two new avenues; revising the method for vessel reconstruction using OCT input rather than micro-CT, or utilising the output of the OCT as a 'ground-truth' to validate the work in this study.

Chapter 6

Conclusion

In order to construct a stented artery computational model, from micro-CT output, a novel method was developed and implemented. This method had 4 key stages; data processing, alignment, suface construction and post-processing. The method as well as its output were assessed in terms of quality and ease of use. This method not only produced the desired model, but also provides a foundation for determining personalised and idealised stent implant techniques for specific patients.

Bibliography

[1] B. Alberts, A. Johnson, J. Lewis, M. Raff, K. Roberts, and P. Walter. *Molecular biology of the cell*. Garland Science, New York, 4 edition, 2002.

[2] L. Antiga, M. Piccinelli, L. Botti, B. Ene-Iordache, A. Remuzzi, and D. A. Steinman. An image-based modeling framework for patient-specific computational hemodynamics. *Medical & Biological Engineering & Computing*, 46(11):1097, Nov 2008.

[3] Australian Institute of Health and Welfare. Australia's Health 2016. Technical Report Cat. no. AUS 199, Australias health series no. 15, Canberra, 2016.

[4] S. Beier. Young researcher improving coronary artery disease treatment, 2017.

[5] L. Bibin, J. Anquez, E. Angelini, and I. Bloch. Hybrid 3D pregnant woman and fetus modeling from medical imaging for dosimetry studies. *International Journal of Computer Assisted Radiology and Surgery*, 5:49–56, 2010.

[6] P. B. Bijari, L. Antiga, D. Gallo, B. A. Wasserman, and D. A. Steinman. Improved prediction of disturbed flow via hemodynamically-inspired geometric variables. *Journal of Biomechanics*, 45(9):1632 – 1637, 2012.

[7] J. Birjiniuk, L. Timmins, M. Young, B. Leshnower, J. Oshinski, and D. Ku. Pulsatile Flow Leads to Intimal Flap Motion and Flow Reversal in an *In Vitro* Model of Type B Aortic Dissection. *Cardiovascular Engineering and Technology*, 8(3):378–389, 2017.

[8] Blender. Shrinkwrap modifier.

[9] F. Bumler, S. Gorb, and S. Bsse. Comparative morphology of the thorax musculature of adult Anisoptera (Insecta: Odonata): Functional aspects of the flight apparatus. *Arthropod Structure Development*, 47(4):430–441, 2018.

[10] T. Bcking, E. Hill, J. Robertson, E. Maneas, A. Plumb, and D. Nikitichev. From medical imaging data to 3D printed anatomical models. *PLOS ONE*, 12(5):1–10, 2017.

[11] Z. Cheng, C. Riga, J. Chan, M. Hamady, N. Wood, N. Cheshire, Y. Xu, and R. Gibbs. Initial findings and potential applicability of computational simulation

of the aorta in acute type B dissection. *Journal of Vascular Surgery*, 57(2-S):35S–43S, 2013.

[12] C. Chiastra, E. Montin, M. Bologna, S. Migliori, C. Aurigemma, F. Burzotta, S. Celi, G. Dubini, F. Migliavacca, and L. Mainardi. Reconstruction of stented coronary arteries from optical coherence tomography images: Feasibility, validation, and repeatability of a segmentation method. *PLOS ONE*, 12(6):1–23, 06 2017.

[13] P. Cignoni, M. Callieri, M. Corsini, M. Dellepiane, F. Ganovelli, and G. Ranzuglia. Meshlab: an open-source mesh processing tool. volume 1, pages 129–136, 01 2008.

[14] M. Collins, X. Li, W. Lv, C. Yang, C. Protack, A. Muto, C. Jadlowiec, C. Shu, and A. Dardik. Therapeutic strategies to combat neointimal hyperplasia in vascular grafts. *Expert Review of Cardiovascular Therapy*, 10(5):635–647, 2012.

[15] K. der Heiden, F. Gijsen, A. Narracott, S. Hsiao, I. Halliday, J. Gunn, J. Wentzel, and P. Evans. The effects of stenting on shear stress: relevance to endothelial injury and repair. *Cardiovascular Research*, 99(2):269–275, 2013.

[16] D. Dillon-Murphy, A. Noorani, D. Nordsletten, and C. Figueroa. Multi-modality image-based computational analysis of haemodynamics in aortic dissection. *Biomechanics and Modeling in Mechanobiology*, 15(4):857–876, 2016.

[17] F. Economou, S. Katranas, G. Giannoglou, K. Gemitzis, I. Styliadis, G. Efthimiadis, H. Karvounis, and A. Ziakas. Impact of stent implantation on endothelial shear stress. *Herz*, 42(5):505–508, Aug 2017.

[18] D. Gallo, D. A. Steinman, and U. Morbiducci. Insights into the co-localization of magnitude-based versus direction-based indicators of disturbed shear at the carotid bifurcation. *Journal of Biomechanics*, 49(12):2413 – 2419, 2016. Cardiovascular Biomechanics in Health and Disease.

[19] E. Grove and S. Kristensen. Stent thrombosis: definitions, mechanisms and prevention. *European Society of Cardiology Council for Cardiology Practice*, 5(32):1–5, 2007.

[20] R. Harper. Drug-eluting coronary stents - a note of caution. *Medical Journal of Australia*, 186(5):253–255, 2007.

[21] C. Hazelaar, M. van Eijnatten, M. Dahele, J. Wolff, T. Forouzanfar, and B. S. Wilko. 3D-Printed Tissue-Mimicking Phantoms for Medical Imaging and Computational Validation Applications. *International Journal of Medical Physics Research and Practice*, 45(1):92–100, 2014.

[22] A. Hruby and F. Hu. The Epidemiology of Obesity: A Big Picture. *Pharmacoeconomics*, 33(7):673–689, 2016.

[23] J. Iqbal, J. Gunn, and P. Serruys. Coronary stents: historical development, current status and future directions. *British Medical Bulletin*, 106(1):193–211, 2013.

[24] M. Kazhdan, M. Bolitho, and H. Hoppe. Poisson Surface Reconstruction. In A. Sheffer and K. Polthier, editors, *Symposium on Geometry Processing*. The Eurographics Association, 2006.

[25] M. Lu, J. Zhao, Y. Guo, J. Ou, and J. Li. A 3d pointcloud registration algorithm based on fast coherent point drift. In *2014 IEEE Applied Imagery Pattern Recognition Workshop (AIPR)*, pages 1–6, Oct 2014.

[26] S. Malek, M. Mosleh, S. Dhillon, and P. Milow. Bioimage Informatics. *Encyclopedia of Bioinformatics and Computational Biology*, 2:993–1010, 2019.

[27] A. Manbachi, Y. Hoi, B. A. Wasserman, E. G. Lakatta, and D. A. Steinman. On the shape of the common carotid artery with implications for blood velocity profiles. *Physiological Measurement*, 32(12):1885–1897, oct 2011.

[28] MedicineNet. Medical definition of thrombosis, 2016.

[29] Medline Plus. Angioplasty and stent placement - heart, 2018.

[30] S. Migliori, C. Chiastra, M. Bologna, E. Montin, G. Dubini, C. Aurigemma, R. Fedele, F. Burzotta, L. Mainardi, and F. Migliavacca. A framework for computational fluid dynamic analyses of patient-specific stented coronary arteries from optical coherence tomography images. *Medical Engineering and Physics*, 47:105–116, September 2017.

[31] S. Minto and F. Remondino. Online access and sharing of reality-based 3D models. *Scientific Research and Information Technology*, 4(2):17–28, 2014.

[32] S. Morlacchi and F. Migliavacca. Modeling Stented Coronary Arteries: Where We are, Where to Go. *Annals of Biomedical Engineering*, 41(7):1428–1444, 2013.

[33] A. Myronenko and X. Song. "point set registration: Coherent point drift". *IEEE Transactions on Pattern Analysis and Machine Intelligence*, 32(12):2262 – 2275, 2010.

[34] U. D. of Commerce. What are imaging phantoms?, 2018.

[35] H. Onishi, M. Hori, T. Ota, A. Nakamoto, K. Osuga, M. Tatsumi, H. Fukui, S. Tsukagoshi, A. Uranishi, Y. Saito, A. Taniguchi, Y. Enchi, K. Sato, and N. Tomiyama. Phantom Study of In-Stent Restenosis at High-Spatial-Resolution CT. *Vascular and Interventional Radiology*, 289(1):92–100, 2018.

[36] J. O'Sullivan, J. Behnsen, T. Starborg, and A. MacDonald. X-ray micro-computed tomography (CT): an emerging opportunity in parasite imaging. *Parasitology*, 145(7):848–854, 2018.

[37] J. Paszkowiak and A. Dardik. Arterial wall shear stress: observations from the bench to the bedside. *Vasc Endovascular Surg*, 37(1):47–57, Jan 2003.

[38] G. Penney, J. Weese, J. Little, P. Desmedt, D. Hill, and D. Hawkes. A comparison of similarity measures for use in 2-D-3-D medical image registration. *IEEE Trans Med Imaging.*, 17(4):586–595, 1998.

[39] N. Ravikumar, A. Gooya, A. Frangi, and Z. Taylor. Generlised Coherent Point Drift for Group-Wise Registration of Multi-dimensional Point Sets. *Medical Image Computing and Computer Assisted Intervention 20th International Conference*, 2017.

[40] S. Manini and L. Antiga. Prepare a surface for mesh generation, 2019.

[41] L. M. Sangalli, P. Secchi, S. Vantini, and A. Veneziani. Efficient estimation of threedimensional curves and their derivatives by freeknot regression splines, applied to the analysis of inner carotid artery centrelines. *Journal of the Royal Statistical Society Applied Statistics Series C*, 58(3):285–306, 2009.

[42] N. Sharma and L. Aggarwal. Automated medical image segmentation techniques. *Jounal of Medical Physics*, 35(1):3–14, 2010.

[43] D. Tihonkih, A. Makovetskii, and V. Kuznetsov. A modified iterative closest point algorithm for shape registration, 2016.

[44] U.S. Department of Health Human Services. Coronary Heart Disease Risk Factors.

[45] K. Valen-Sendstad, K.-A. Mardal, and D. A. Steinman. High-resolution cfd detects high-frequency velocity fluctuations in bifurcation, but not sidewall, aneurysms. *Journal of Biomechanics*, 46(2):402 – 407, 2013. Special Issue: Biofluid Mechanics.

Appendix A

This section contains the data produced from the evaluation simulations described in Chapter 4.

A.1 CPD Simulation Output

Iterations	Alignment	RMSE	Iterations	Alignment	RMSE
1	CPD	0.636407637	17	CPD	0.525386318
2	CPD	0.752192402	18	CPD	0.508747566
3	CPD	0.753429838	19	CPD	0.491447817
4	CPD	0.739960305	20	CPD	0.472929625
5	CPD	0.724904401	21	CPD	0.453393632
6	CPD	0.707288089	22	CPD	0.432952308
7	CPD	0.690597125	23	CPD	0.411696919
8	CPD	0.674835601	24	CPD	0.389847474
9	CPD	0.659259564	25	CPD	0.36797732
10	CPD	0.643323008	26	CPD	0.346410912
11	CPD	0.627162229	27	CPD	0.32528733
12	CPD	0.610407389	28	CPD	0.304408544
13	CPD	0.593321659	29	CPD	0.28459381
14	CPD	0.576086149	30	CPD	0.26496497
15	CPD	0.558927158	31	CPD	0.245399049
16	CPD	0.541961508			

A.2 ICP Simulation Output

Iterations	Alignment	RMSE	Iterations	Alignment	RMSE
1	ICP	1.889282974	17	ICP	1.426150426
2	ICP	1.555684902	18	ICP	1.426150426
3	ICP	1.47520547	19	ICP	1.426150426
4	ICP	1.44882397	20	ICP	1.426150426
5	ICP	1.437160243	21	ICP	1.426150426
6	ICP	1.4314327	22	ICP	1.426150426
7	ICP	1.428810149	23	ICP	1.426150426
8	ICP	1.42735156	24	ICP	1.426150426
9	ICP	1.426721561	25	ICP	1.426150426
10	ICP	1.42641708	26	ICP	1.426150426
11	ICP	1.426277063	27	ICP	1.426150426
12	ICP	1.426202858	28	ICP	1.426150426
13	ICP	1.426166763	29	ICP	1.426150426
14	ICP	1.426150426	30	ICP	1.426150426
15	ICP	1.426150426	31	ICP	1.426150426
16	ICP	1.426150426			

Appendix B

The data produced from a similarity simulation, described in Chapter 4

B.1 Similarity Simulation

Input	Vessel	Stent
Previous Work	5.344	1.4052
Growth Approach	3.519	0.8153
Novel Approach	1.2456	0.6552
Stent	2.6763	0
Vessel	0	0.7635